



INVESTIGATION OF THE USE OF THE RESIDUAL DRIFT FOR POST-EARTHQUAKE ASSESSMENT OF DAMAGED RC STRUCTURES

K. Dai⁽¹⁾, J. Wang⁽²⁾, Y. Xu⁽³⁾, B. Li⁽⁴⁾, and H. Zhang⁽⁵⁾

⁽¹⁾ Associate Professor, State Key Laboratory of Disaster Reduction in Civil Engineering, Tongji University, and Adjunct Faculty, State Key Laboratory for GeoMechanics and Deep Underground Engineering, kdai@tongji.edu.cn

⁽²⁾ Research Assistant, State Key Laboratory of Disaster Reduction in Civil Engineering, Tongji University, wangdongkid@126.com

⁽³⁾ Research Assistant, State Key Laboratory of Disaster Reduction in Civil Engineering, Tongji University, xyz_ahbb@163.com

⁽⁴⁾ Research Assistant, State Key Laboratory of Disaster Reduction in Civil Engineering, Tongji University, 360181349@qq.com

⁽⁵⁾ Research Assistant, State Key Laboratory of Disaster Reduction in Civil Engineering, Tongji University, tjzhanghexiao@163.com

Abstract

Post-earthquake assessment of damaged structures is one of important tasks for civil engineers after a seismic event. For conventional buildings, the residual drift is a permanent deformation that a building structure sustains after strong ground shaking. This residual drift is usually one of measurable information in post-earthquake reconnaissance. It has been studied as one of post-earthquake damage assessment indices. In this paper, an example of field measurement of residual drift was introduced to reflect the difficulty of using residual drift alone to classify damage of a building after earthquake. Two kinds of approaches used to estimate peak drift based on residual drift are reviewed. However, these approaches have not been fully assessed by experimental data. A shaking table test of a full-scale four-story RC structure model was used as a case to assess the proposed peak drift estimation methods. Analysis results indicate that the probabilistic inference method that incorporates uncertainties is recommended to be used in practical engineering cases.

Keywords: seismic assessment, residual drift, LiDAR measurement, shaking table testing validation

1. Introduction

After strong earthquakes, seismic capacity assessment of damaged structures is one of important tasks for civil engineers. An accurate assessment is critical for a sound decision making regarding post-earthquake usability and/or reparability of buildings. The peak inter-story drift or roof drift of a building is usually employed as a primary index to assess structural performances of post-earthquake buildings (e.g., [1-3]). However, the seismic peak drift sustained by the building can only be measured if a structural health monitoring system is already installed in place prior to the earthquake occurrence, which is not yet a common practice for most buildings. Often the residual drift or permanent deformation of a building is measured in-situ after strong earthquakes as one of indices in structural seismic assessment. Various new techniques, such as 3D laser scanning [4, 5], digital image correlation method [6], the global positioning system (GPS) [7, 8], and the use of robotic theodolites (RTS) [9], have been developed to facilitate on-site residual drift measurement.

Investigating the direct use of the residual drift or residual inter-story drift of structures to quantify and classify seismic damage can be found in the literature [10, 11]. However, statistical analyses indicated that the residual drift is significantly affected by ground motion intensity, site condition, as well as structural properties, especially the hysteretic behaviors [12-14]. It is a common conclusion that the residual drift has a very large scatter (i.e., large coefficient of variation (CoV)) due to record-to-record variability [12]. The peak inter-story drift or roof drift of a building is a more reliable damage index in seismic assessment. However, due to the difficulties in directly obtaining the peak drift, it is of interest to predict the peak drift based on the measurable residual drift for a building that sustained an earthquake.



The methods in the available studies can generally be classified as the empirical relation based (deterministic) method and the probabilistic inference based method. One of the approaches to estimate the peak drift is to use an empirical relation between the residual drift and the peak drift [15-20]. Instead of using empirical relations to predict a single value of peak drift based on the observed residual drift, assessments of the probability distribution of peak drift conditioned on the observed residual drift were considered for equivalent SDOF systems [21] and for structural members that were tested on a shaking table [22].

In this paper, a field testing for residual drift measurement of a seismic damaged structure was first briefly introduced to understand difficulties in directly evaluating structural damages purely based on the residual drift. With the purpose to perform damage assessment, the aforementioned two approaches, empirical relations and the probabilistic method for predicting peak drift based on the measured residual drift were reviewed and assessed by a full-scale building tested on a shaking table. The estimated values derived from these two methods were compared with the shaking table test measurements.

2. Field Measurement of a Seismic Damaged Structure

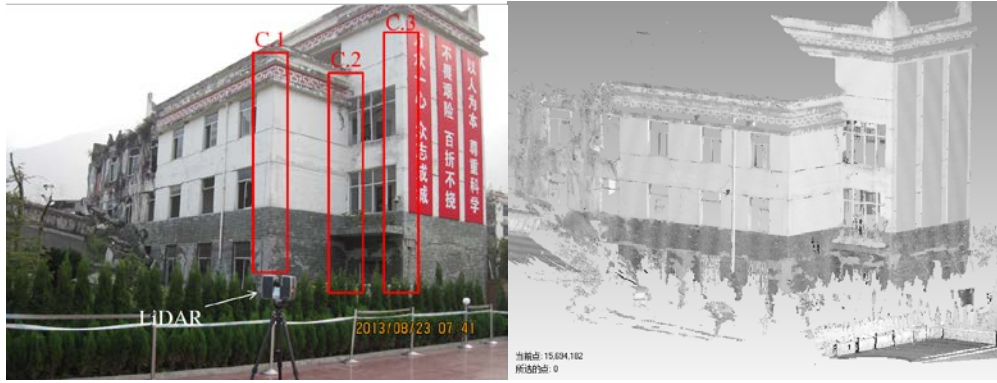
With recent advances in hardware and software of laser scanning system, terrestrial LiDAR was explored for building geometrical profile measurement of a subject. The terrestrial LiDAR technology is able to provide 3D point cloud data with a high spatial resolution of a millimeter level. It is possible to use the LiDAR technology to measure residual drifts of damaged buildings after earthquake. The uniqueness of this technology is that the residual drift can be measured remotely, therefore, reducing dangers for field inspectors and engineers. A pilot study was conducted to use this technology for field investigation of buildings damaged in the Wenchuan earthquake and an example work was briefly introduced in this manuscript with an objective of helping understand difficulties in directly evaluating structural damages purely based on the residual drift.

The Wenchuan earthquake occurred in Sichuan province, China on 12 May 2008. It resulted in millions people homeless and caused huge economic losses. The Xuankou secondary school was located near the epicenter of the earthquake. School buildings were severely damaged in earthquakes. An example building is shown in Fig. 1a. It is a typical RC moment-frame structure building consisting of four storeys. A global building deformation relative to the ground level induced by seismic loads could be observed in site investigation clearly. With the LiDAR technology, this damaged building was scanned as shown in Fig. 1(b). The inter-storey residual drifts were estimated along three corners, which circled with red color lines in Fig 1a as C1, C2, and C3. Three residual drifts for each storey were calculated based on LiDAR scanning information and a total of nine values were derived. The maximum and minimum residual drift values along these three wall corners for each storey were summarized in Table 1.

The measured residual drift could be used directly to classify the damage states of this damaged building. According to the performance level classifications of RC structures defined in FEMA-356 [1] as shown in Table 2, the seismic damage of the building is beyond the “Life Safety” if the maximum values in Table 1 are considered. However, the state of “Immediate Occupancy” could also be tagged based on the minimum values in Table 1. This large difference between maximum and minimum values reflects the complexity of using the residual drift alone to classify damage or performance levels in seismic assessment of a building structure. The peak inter-story drift or roof drift of a building is believed to be a more reliable damage index. However, it is difficult to directly measure the peak drift if a structural health monitoring system is unavailable. Therefore, it is of interest to predict the peak drift based on the measurable residual drift. Existing approaches were investigated and evaluated through a full-scale shaking table test in the following.

Table 1 – Measured residual drift of the damaged building for each storey

Item	1st storey	2nd storey	3rd storey	4th storey
Maximum	1.41%	1.57%	1.38%	1.60%
Minimum	0.49%	0.54%	0.82%	0.63%



(a) Damaged building photo

(b) Scanned point cloud of the building

Fig. 1 – Damaged building and scanned point cloud

Table 2 – Performance levels of drift limitations in [1].

Item	Collapse Prevention	Life Safety	Immediate Occupancy
Peak drift	4%	2%	1%
Residual drift	4%	1%	Negligible permanent

3. Methods for Peak Drift Estimation Based on Residual Drift

3.1 Empirical relations for predicting the peak displacement

Five existing empirical relations between the peak and residual displacement found in the literature were summarized in Table 3. These equations were established from extensive numerical analyses, considered the uncertainties associated with structural properties and seismic inputs. Among these relations, Eqs. (2) and (3) [16] were developed for the SDOF systems with Takada and Kinematic hysteresis models, respectively. Eq. (5) [18] could be applied to a multi-degree of freedom (MDOF) system representing a regular multi-storey structure with a symmetrical layout. The regression analyses to determine model coefficients in Eq. (5) was based on the minimization of absolute residual error using “the Pearson VII limit” (i.e., minimum sum of $\ln[(1+\text{residual}^2)^{1/2}]$); the maximum displacements predicted by using Eq. (5) were significantly scattered [18].

3.2 Inference based on the probabilistic framework

A procedure based on the Bayesian theorem to estimate the damage probability using the post-earthquake observations was proposed in [22], which considered the uncertainties in the structural dynamic responses caused by ground motions. In summary, this procedure for a building that sustained a seismic event can be described as:

(1) The prior probability density function of the peak drift for the building $f(\theta_p)$ is assigned based on the structural analyses results of the building under the considered seismic event. Actual ground motion records at the building site should be used. If the record is unavailable, it is suggested to infer ground motions from the records at stations close to the building site for the considered event or, to produce simulated ground motions based on characteristics that are compatible to the considered event. This, however, increases the uncertainty in the assigned probability distribution.

(2) Updating the probability distribution of peak drift, θ_p , based on structural damage observations and residual drift measurements. This can be expressed as,

$$f(\theta_p | I \cap \theta_r) \propto f(I \cap \theta_r | \theta_p) f(\theta_p) \quad (6)$$



where I denotes all observed and/or measured damage information, θ_r denotes the residual drift, $f(\theta_p | I \cap \theta_r)$ is the updated probability density function of θ_p and $f(I \cap \theta_r | \theta_p)$ is the joint probability density function of the observed damage and residual drift conditioned on θ_p .

Within this probabilistic framework, the residual drift measurement is used as one of the indices to update the probability distribution of the peak drift. Unlike the deterministic approaches, Eq. (6) provides a probabilistic estimation of the peak drift which acknowledges the uncertain relation between the residual and peak drifts.

Table 3 – Empirical relations between the maximum and residual displacements.

References	Equation
[15, 23]	$u_e = u_r / \left\{ \left[\frac{1}{\theta_1} + \frac{1}{41T_n^{\theta_2}} \right] \left[1 - \exp(-\theta_4(R-1)^{\theta_5}) \right] \theta_3 \right\} \quad (1a)$ $u_p = u_e \cdot \left\{ 1 + \left[\frac{1}{a_1(T_n/T_s)^{a_2}} - \frac{1}{a_3} \right] (R-1) \right\} \quad (1b)$
[16]	$u_r = \left(\frac{0.019}{a_g^{1/3}} \right) \{ \exp[10[(1-r) \frac{u_p}{u_y} + (r-1)u_p u_y]] - 1 \} \quad (2)$
	$u_r = \left(\frac{0.00074}{a_g^{5/6}} \right) \{ \exp[35[(1-r) \frac{u_p}{u_y} + (r-1)u_p u_y]] - 1 \} \quad (3)$
[17]	$u_r = \frac{u_p - u_y}{[-0.069a_g^2 + 1.164a_g] \times 10^2 r + 3.58} \quad (4)$
[18]	$u_p = (a_1 + a_2 u_r + a_3 u_r^2 + a_4 T_n u_r) \times (1 + a_5 r + a_6 r^2) \quad (5)$

Note: u_r and u_p are the residual and the peak displacements, respectively; u_e is the recoverable elastic drift; T_n is the fundamental vibration period of the structure; T_s is the characteristic period of the site; r is the post-yielding stiffness ratio; R is the lateral strength ratio, defined as $R = mS_a/F_y$, where m is the mass of the system, S_a is the acceleration spectral, and F_y is the lateral yielding strength of the system; a_1 - a_6 and θ_1 - θ_5 are fitted parameters that depend on site conditions; and a_g is the peak ground acceleration (PGA).

4. Shaking Table Test Validation

4.1 Shaking table test and numerical modelling

A series of shaking table tests were conducted on a full-scale, four-story building on the National Research Institute for Earth Science and Disaster Prevention (NIED) E-Defense shaking table in December 2010 [24]. The test building was a conventional reinforced concrete (RC) building. The test building adopted two-bay moment frames in the longitudinal direction (X) and two structural walls, at each end of the building plan, in the transverse direction (Y). The building height is 12 meters with 3 meters story height for each floor. The input ground motions during the test are the JMA-Kobe ground motions (recorded in 1995) that are scaled with a scaling factor of 25%, 50%, and 100%. The test building was instrumented with accelerometers, displacement transducers and strain gauges and thus peak and residual roof drift results could be obtained [24]. In the JMA-Kobe-100% test case (i.e., recorded ground motions), 0.08% residual roof drift and more evident structural damage were observed for the moment frame in the X direction. The test results from this loading scenario were used to assess the adequacy of the aforementioned two approaches in predicting the peak roof drift.

In this study, a 3D finite element (FE) model of the test building was developed with commercial software, Perform-3D [26]. In this model, columns were modeled with inelastic fiber sections and the nonlinear behaviors of beams were modeled with moment-rotation plastic hinges. The plastic hinge length were estimated according to the recommendations given in [27]. For the material properties, unconfined concrete and reinforcing steel stress-strain relations were defined with trilinear relationships based on the results of material tests that were performed prior to the shaking table test [24]. Parameters for the confined concrete were defined based on

the method proposed in [28]. The Rayleigh damping of 2.5% at $0.2 T_n$ and $1.0 T_n$, where T_n is the period of the first vibration mode, was used for the nonlinear response history analyses with the recommendation in [29]. The mass, lumped at every beam-column joint resulting from its tributary area, was estimated based on the weight of the structures reported in [24].

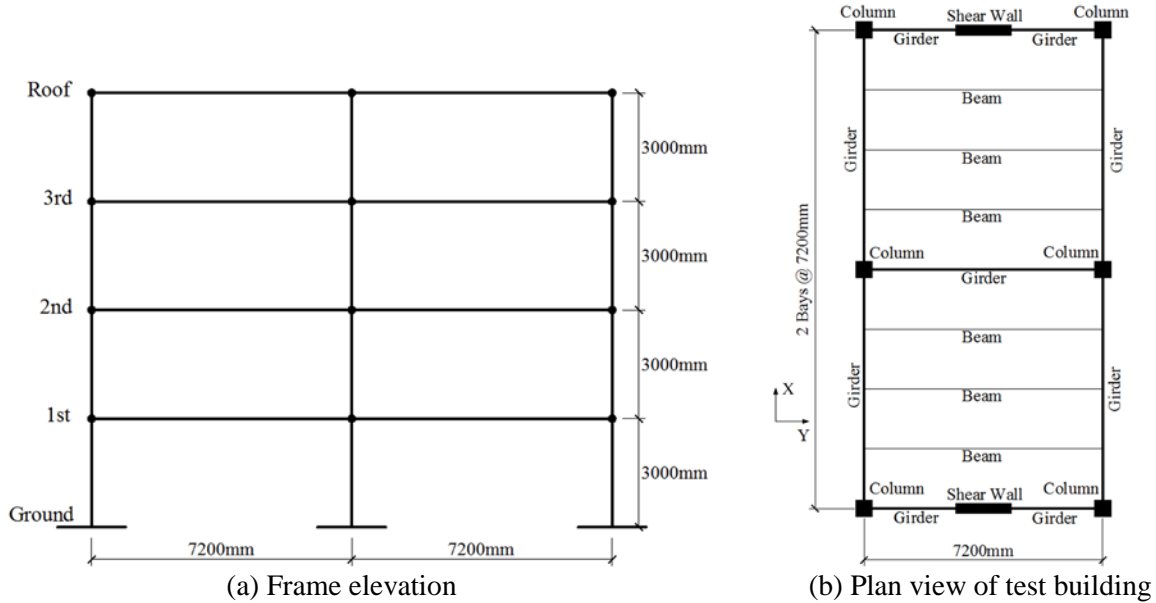


Fig. 2 – Elevation and plan views of the test building.

Time history analyses were performed for the developed FE model with the same scaled JMA-Kobe ground motions used for the full scale test. A 5-s duration zero-amplitude acceleration time history was added at the end of each time history, allowing the residual drift to be identified after the actual excitations. Since the test results did not show a strong coupling in [30], only the test results along the X-direction as well as the calculated responses subjected to the ground motions along X-direction were considered in the following part of this study. The calculated roof drift time histories for the scaled JMA-Kobe ground motions were compared to the full-scale test results as shown in Fig. 3. A good agreement between the test and numerical results presented in the figures indicated the adequacy of the FE model in capturing global responses of the building. Therefore, this validated FE model was used in the following to calculate structural responses under seismic excitations.

4.2 Peak drift prediction based on empirical relations

The empirical equations listed in Table 3 were applied to predict the peak displacements based on the residual displacement. Structural properties required in the equations including the post-yielding stiffness ratio r and the yielding displacement u_y were estimated through the static pushover analysis by using the developed FE model as illustrated in Fig. 4. The residual roof drift of $\theta_r = 0.08\%$ ($u_r = 10$ mm) after the JMA-Kobe-100% test case was considered as the measured value to estimate the peak roof drift by using the equations shown in Table 3. To calculate the lateral strength ratio R ($R = mS_a / F_y$) in Eq. (1), the test building was simplified as an equivalent SDOF system with the equivalent mass m , which was obtained from the modal mass of the first mode multiplying the modal participation factor of this mode; the spectral acceleration (S_a) of the JMA-Kobe at the fundamental period of the test structure ($T_n=0.69$ s), S_a , which equals $1.91 g$ (g is the gravitational acceleration); and the yielding lateral strength $F_y=1756$ kN, which was estimated from pushover analysis results shown in Fig. 4. The horizontal top drift of the equivalent SDOF system for Eqs. (1) to (4) were obtained by dividing the measured roof drift by the height of the building. Eq. (5) was directly applied to the test building since it was indicated [18] that it can be applied to multi-story structures. Note that the parameters $\theta_1-\theta_5$, a_1-a_3 in Eq. (1) and a_1-a_6 in Eq. (5) were selected for the site condition D (stiff soil) in [31], representing the site condition where the JMA-Kobe record was recorded.

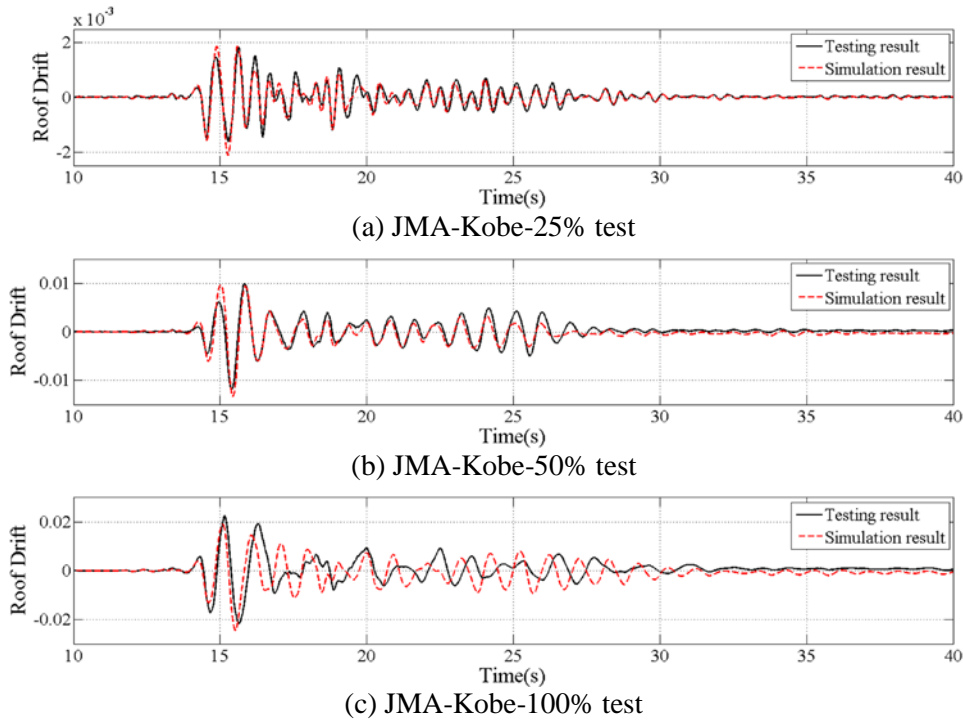


Fig. 3 – Roof drift time-history comparisons between testing and simulation results.

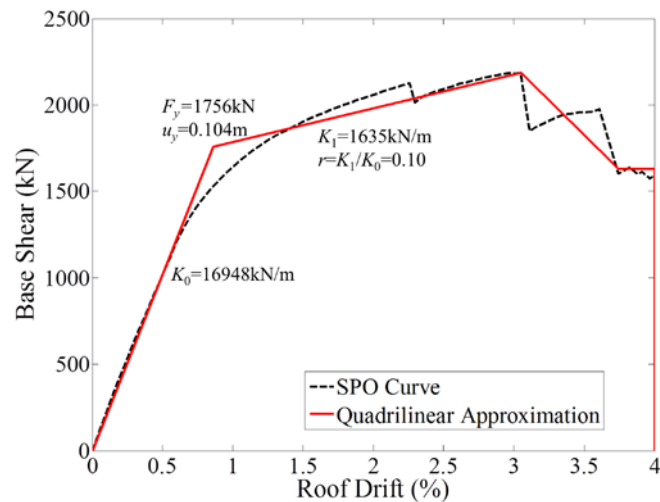


Fig. 4 – Static pushover curve.

The peak roof displacements estimated by using Eqs. (1) to (5) were compared with the test results of peak displacements $u_p = 272$ mm in Table 4. The comparison indicates that Eqs. (1) and (5) underestimate the peak roof displacement significantly. Eq. (2), which is based on the Takada model, shows a better performance than Eq. (3), which is based on the Kinematic model. For the best prediction of 250 mm given by Eq. (4), the corresponding relative difference between the estimated and measurement is 8%. However, these observations were based on the comparisons between calculated and test results for a single test building under the JMA-Kobe ground motion. It was also indicated in [18] that Eq. (5) was applied successfully for a RC frame, but it did not provide a reliable estimation for the test building as shown in Table 4. This may be attributed to the fact that the pinching-effect or hysteric behavior of the RC structure in [18] are different from those of the test building. Therefore, whether an empirical equation can provide a satisfactory estimation of the peak displacement for different structures or under different earthquake excitations was uncertain. In general, these comparisons



indicate that the use of the empirical models together with observed residual displacement to assess the peak displacement (i.e., the post-earthquake damage) could be associated with large variability.

Table 4. Comparison between the test results and the empirical equation estimations.

Empirical equation	Calculated peak displacement (mm)	Relative Difference
(1)	18	94%
(2)	227	20%
(3)	218	25%
(4)	250	8%
(5)	72	73%

Note: $Relative\ Difference = (u_{exact} - u_{evaluated}) / u_{exact} \times 100\%$

4.3 Peak drift prediction based on probabilistic inference method

Prior to the use of the probabilistic method, it was assumed that the peak roof drift θ_p obtained from the test building is unavailable. Following the main steps of briefly described in Section 3.2, a set of the peak roof drift intervals ma_i for the peak roof drift distribution of θ_p was firstly established for the considered seismic event by dividing the drift range from 0 to 4% with an interval of 0.25%, where

$$M_i = \{ma_i < \theta_p \leq ma_{i+1}\} \quad (7)$$

in which $ma_i = 0.25\% \times (i - 1)$, $i = 1, 2, \dots, 17$. The adoption of the upper limit of 4% for the peak roof drift is based on the ‘‘Collapse Prevention’’ drift limits in Table 2. The bin width of 0.25% was employed to be consistent with the value employed in [22].

Similarly, the residual drift θ_r was defined within the following bins or events R_j ,

$$R_j = \{ra_j < \theta_r \leq ra_{j+1}\} \quad (8)$$

where $ra_j = 0.05\% \times (j - 1)$, $j = 1, 2, \dots, 7$. By treating the peak roof drift and the residual drift as discrete events rather than continuous random variables, numerical analyses for the probability updating can be simplified.

In addition, the structural modelling error was ignored in the probabilistic analysis since geometrical and material information of the structure [24], being collected in the laboratory environment, is believed to be relatively reliable. However, it should be noted that this assumption may not be suitable for field investigation cases. For the ground motion inputs, two cases described below were investigated.

Case 1: It was assumed that the ground motions (i.e., the JMA-Kobe record) for the considered earthquake (defined by magnitude and source to site distance) were recorded at a site close to the building. However, the station is not exactly installed at the building site. The JMA-Kobe event is defined by the moment magnitude $M_w = 6.9$, the Joyner-Boore distance $R_{jb} = 0.94$ km, and the closet distance to rupture $R_{rup} = 0.96$ km. In the PEER NGA database, besides the JMA-Kobe record, no other record was found for the same magnitude and distance characteristics. To include more ground motion records that could resemble the ground motions at the building site for the specific seismic event, records were selected from PEER NGA database based on: (a) Moment magnitude is within 6.0 to 8.0; and (b) R_{jb} is less than 5 km, and R_{rup} ranges 0 to 4.38 km. A set of 50 ground motion records was selected and each of the selected records was scaled to have $S_a = 1.91$ g at $T_n = 0.69$ s, which represent the S_a at $T_n = 0.69$ s for the JMA-Kobe record. The spectra of the scaled records for Case 1 were shown in Fig. 5a.

Case 2: There are no ground motion time history records available close to the building site after an earthquake. However, the magnitude or intensity of the seismic event as well as the design spectrum for the building are available. The test building was designed to be located in a region where the mapped short period and 1-sec-period accelerations are 1.5 g and 0.9 g, respectively, and $T_s = 0.6$ s for Site Class B in [31]. The design response spectrum of the maximum considered earthquake (MCE) for the full-scale test building was constructed following the recommendation in [31]. The S_a of the MCE is 1.32 g at $T_n = 0.69$ s and the damping



ratio of 5%. Ten ground motion records for the site class B were selected from the PEER NGA database [32]. Five records with pronounced velocity-pulse characteristics and the remaining five records without pronounced velocity-pulse characteristics were selected in order to give the same weight to pulse and non-pulse types of ground motions. The response spectra of the scaled records with $S_a = 1.32$ g at $T_n = 0.69$ s were presented in Fig. 5b. Since the S_a at $T_n = 0.69$ s for the building site was assumed to be unknown for this case, the S_a at $T_n = 0.69$ s for the building site is modeled as a lognormal variate with a median equal to 1.32 g, and the standard deviation of the natural logarithm of the S_a at $T_n = 0.69$ s was estimated as 0.58 based on the ground motion prediction equation developed in [33]. The value is within the range suggested in [34] by considering the interevent variability only and by considering the overall variability. Based on the above criteria, 20 S_a values ($T_n = 0.69$ s) were considered and each component of the ground motion record selected from PEER NGA database was scaled to match the target S_a values. A total of 200 time history analyses were therefore conducted for this case.

For these two cases, the prior probability distributions of the peak roof drift $P(M_i)$ were assigned based on the results of nonlinear inelastic time-history analyses by using the testing building FE model. The assigned distributions are shown in Fig. 6. The distribution modes for Case 1 and Case 2 are different: the most likely peak roof drifts fall approximately into the ranges of 2.25% - 2.5% or 1.5% - 1.75% for Case 1 and Case 2, respectively. The peak roof drift for Case 1 is closer to the measured value (2.27%) since the reference ground motion information is available for this case.

It was noted in [25] that after the JMA-Kobe-100% test case, the observed damage of the 1st and 2nd stories of the test building is between “Life Safety” and “Collapse Prevention” described in the FEMA-356 [1]. The damages of the 3rd and 4th stories were less severe, which should be classified as “Life Safety”. Accordingly, the inter-story drifts of first two stories were assumed in the range of 2% to 4% and the inter-story drifts of the 3rd and 4th stories were assumed in the range of 1% to 2%. Therefore, the peak roof drift of the building subjected to 100% of the JMA-Kobe record was then assumed to be in the range of 1% to 4%.

Let the event I_1 represent the scenario that the observed damage of each story is more severe than the damage state of “Immediate Occupancy” defined in [1]. Similarly, let the event I_2 represent the damage state in each story that is in the state or beyond the state of “Collapse Prevention”. The peak roof drift distribution conditioned on the observed “damage state” I , $P(M_i|I)$, can be calculated by using,

$$P(M_i|I_1) = \frac{P(I_1|M_i)P(M_i)}{\sum_j P(I_1|M_j)P(M_j)} \quad (9a)$$

$$P(M_i|I_1 \cap \bar{I}_2) = \frac{P(\bar{I}_2|M_i \cap I_1)P(I_1|M_i)}{\sum_j P(\bar{I}_2|M_j \cap I_1)P(I_1|M_j)} \quad (9b)$$

It was reasonable to consider that the damage severity of a structure is an increasing function of its peak drift. However, there is no widely-accepted probability model to describe the relation between structural damages and the peak drift. Therefore, for simplicity, in Eq. (9), the probability distribution of $P(I_1|M_i)$ and $P(\bar{I}_2|M_i \cap I_1)$ were assumed to be uniform in the range of 1% to 4%, and the values of $P(I_1|M_i)$ and $P(\bar{I}_2|M_i \cap I_1)$ are the cumulative probability at the value of mc_i , where $mc_i = (ma_{i+1} + ma_i)/2$.

Likewise, the observed damage was used in updating $P(M_i \cap R_j|I)$ based on,

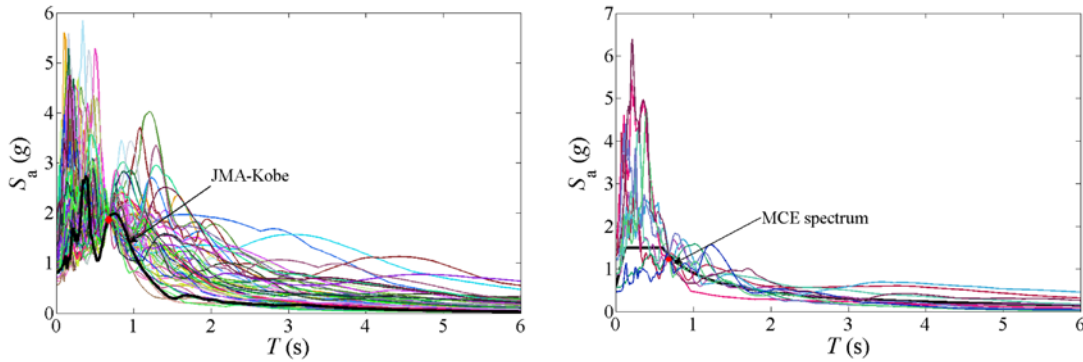
$$P(M_i \cap R_j|I_1) = \frac{P(I_1|M_i \cap R_j)P(M_i \cap R_j)}{\sum_m \sum_n P(I_1|M_m \cap R_n)P(M_m \cap R_n)} \quad (10a)$$

$$P(M_i \cap R_j | I_1 \cap \bar{I}_2) = \frac{P(\bar{I}_2 | M_i \cap R_j \cap I_1) P(M_i \cap R_j | I_1)}{\sum_m \sum_n P(\bar{I}_2 | M_m \cap R_n \cap I_1) P(M_m \cap R_n | I_1)} \quad (10b)$$

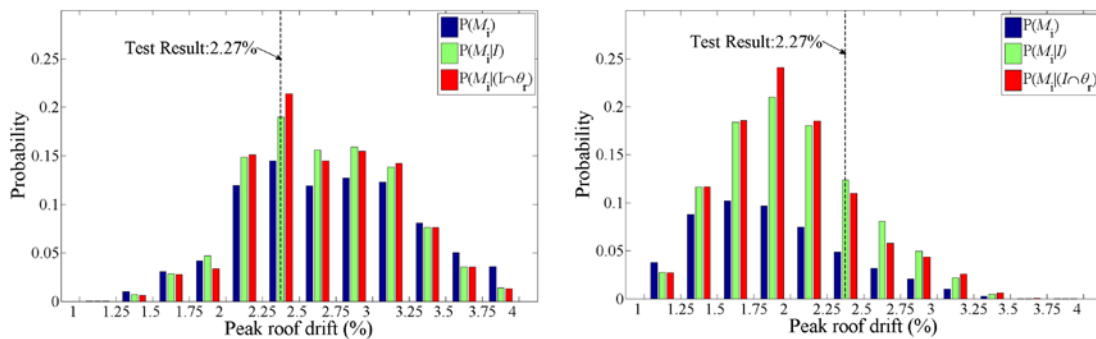
Although the probabilistic model of $P(I_1 | M_i \cap R_j)$ and $P(\bar{I}_2 | M_i \cap R_j \cap I_1)$ are not well established, the tendency is widely accepted that a large residual drift usually indicates more severe structural damages under a condition of a specific peak drift. To simplify the problem in this study, $P(I | M_i \cap R_j)$ was assumed to be given by,

$$P(I_1 | M_i \cap R_j) = P(I | M_i) \times j / \sum_j \quad j=1,2,\dots,6,7 \quad (11a)$$

$$P(\bar{I}_2 | M_i \cap R_j \cap I_1) = P(\bar{I}_2 | M_i \cap I_1) \times (8 - j) / \sum_j \quad j=1,2,\dots,6,7 \quad (11b)$$



(a) Case 1 (b) Case 2
Fig. 5 – Acceleration response spectra (5% damping).



(a) Case 1 (b) Case 2
Fig. 6 – Probability distributions of the peak roof drifts.

In addition, the probability distribution of the peak roof drift conditioned on both the measured residual roof drift and the observed damage, $P(M_i | I \cap \theta_r)$, can be estimated using Eq. (12) [22]:

$$P(M_i | I \cap \theta_r) = \sum_j \frac{P(M_i \cap R_j | I)}{P(R_j | I)} P(R_j | \theta_r) \quad (12a)$$

$$P(R_j | I) = \sum_k P(M_i \cap R_j | I) \quad (12b)$$



With these equations and the residual roof drift $\theta_r = 0.08\%$ ($u_r = 10$ mm) that was measured for the JMA-Kobe-100% test case, the calculated $P(M_i|I)$ and $P(M_i|I \cap \theta_r)$ are shown in Fig. 6. From the figures, it can be observed that for Case 1, the drift interval associated with the maximum probability (mass) is 2.25% - 2.5% and it shows a good agreement with the test result of 2.27%. For Case 2, after the Bayesian updating drift range associated with the maximum probability (mass) shifted from 1.5% - 1.75% to 1.75% - 2%. However, the values within this interval are still smaller than the measured peak roof drift (2.27%). The reason may attribute to the larger uncertainty in the ground motions than that in Case 1. Moreover, the mean and median values of $P(M_i|I \cap \theta_r)$ are 2.65% and 2.39% for Case 1; 1.98% and 1.67% for Case 2, respectively. The median value of Case 1 is only 5.3% different from the testing result.

5. Conclusions

An example of field measurement for residual drift of a seismic damaged structure using laser scanning technique was first introduced. It indicated that the direct use of the measured residual drift information in seismic assessment shows large uncertainties. Since the peak drift is believed to be more reliable than the residual drift as an index for evaluating building performance, this paper investigated the use of two approaches to estimate the peak drift based on the measured residual drift: (1) predicting the peak drift from the residual drift using an empirical model; (2) evaluating the peak drift distribution based on probabilistic inference considering the observed and measured damage indications.

Results of a full-scale four-story RC building were used as a case study to assess both approaches. The results showed that, only one of the five considered empirical equations provided a close prediction of the peak roof drift response obtained from laboratory tests. Whether this observed adequate prediction is valid for other buildings or under different earthquake excitations was unknown. This was partly due to the record-to-record variability. The probabilistic method for the peak drift estimation with the consideration of visible damages and measurable residual displacements was also investigated in this study. This method allowed a joint treatment of subjective and objective information for damage evaluation. A rational selection of the probability distribution models was found to be the key to improve the effectiveness of the probabilistic method. The probabilistic approach considers the uncertainties involved in earthquake events. Since the residual displacement is sensitive to the model error dispersion and record-to-record variability, this approach is expected to be a logical framework.

6. Acknowledgements

The authors would like to acknowledge the support from the State Key Laboratory of Disaster Reduction in Civil Engineering (Grant No. SLDRCE14-B-02), and State Key Laboratory for GeoMechanics and Deep Underground Engineering (Grant No. SKLGDUEK1514). The preliminary work of Mr. Kai Lu of Tongji University in the early stage of this study is also acknowledged.

7. References

- [1] FEMA 356 (2000): *Prestandard and commentary for the seismic rehabilitation of buildings*. Federal Emergency Management Agency, Washington, DC.
- [2] FEMA P-58 (2012): *Seismic performance assessment of Buildings*. Federal Emergency Management Agency, Washington, DC.
- [3] FEMA P-750 (2009): *NEHRP Recommended seismic provisions for new buildings and other structures*. Federal Emergency Management Agency, Washington, DC.
- [4] Yang L, Sheng Y, Wang B (2016): 3D reconstruction of building facade with fused data of terrestrial LiDAR data and optical image. *Optik-International Journal for Light and Electron Optics*, **127**(4), 2165-2168.



- [5] Canaz S, Karsli F, Guneroglu A, Dihkan M (2015): Automatic boundary extraction of inland water bodies using LiDAR data. *Ocean & Coastal Management*, **118**, 158-166.
- [6] Quan C, Tay CJ, Huang YH (2004): 3-D deformation measurement using fringe projection and digital image correlation. *Optik-International Journal for Light and Electron Optics*, **115**(4), 164-168.
- [7] Lovse JW, Teskey WF, Lachapelle G, Cannon ME (1995): Dynamic deformation monitoring of tall structure using GPS technology. *Journal of surveying engineering*, **121**(1), 35-40.
- [8] Nickitopoulou A, Protopsalti K, Stiros S (2006): Monitoring dynamic and quasi-static deformations of large flexible engineering structures with GPS: accuracy, limitations and promises. *Engineering Structures*, **28**(10):1471–1482.
- [9] Psimoulis P, Stiros S (2007): Measurement of deflections and of oscillation frequencies of engineering structures using robotic theodolites (RTS). *Engineering Structures*, **29**(12), 3312–3324.
- [10] Toussi S, Yao JTP (1983): Hysteresis identification of existing structures. *Journal of Engineering Mechanics*, **109**(5): 1189–1203.
- [11] Stephens JE, Yao JTP (1987): Damage assessment using response measurements. *Journal of Structural Engineering*, **113**(4), 787–801.
- [12] Mahin SA, Bertero VV (1981): An evaluation of inelastic seismic design spectra. *Journal of Structural Division*, **107**(9), 1777–1795.
- [13] Uma S, Pampanin S, Christopoulos C (2010): Development of probabilistic framework for performance-based seismic assessment of structures considering residual deformations. *Journal of Earthquake Engineering*, **14**(7),1092-1111.
- [14] Liossatos E, Fardis MN (2014): Residual displacements of RC structures as SDOF systems. *Earthquake Engineering and Structural Dynamics*, **44**(5), 713–734.
- [15] Ruiz-García J, Miranda E (2006): Residual displacement ratios for assessment of existing structures. *Earthquake Engineering and Structural Dynamics*, **35**(3), 315-336.
- [16] Gong JX, Cheng L, Zhang Q (2011): Statistical relationship between results of static nonlinear analysis and elasto-plastic time-history and calculation of residual deformation for structures. *Journal of Building Structures*, **32**(12), 224-233. (in Chinese)
- [17] Zhang Q, Zhu J, Gong J (2013): Post-earthquake residual deformation prediction of SDOF system. *Journal of Civil, Architectural and Environmental Engineering*, **35**(3), 32-41. (in Chinese)
- [18] Hatzigeorgiou GD, Papagiannopoulos GA, Beskos DE (2011): Evaluation of maximum seismic displacements of SDOF systems from residual deformation. *Engineering Structures*, **33**(12), 3422–3431.
- [19] Christidis AA, Dimitroudi EG, Hatzigeorgiou GD, Beskos DE (2013): Maximum seismic displacements evaluation of steel frames from their post-earthquake residual deformation. *Bulletin of Earthquake Engineering*, **11**(6), 2233-2248.
- [20] Erochko J, Christopoulos C, Tremblay R, Choi H (2011): Residual drift response of SMRFs and BRB frames in steel buildings designed according to ASCE 7–05. *Journal of Structural Engineering*, **137**(5), 589–599.
- [21] Goda K (2010): Statistical modeling of joint probability distribution using copula: application to peak and permanent displacement seismic demands. *Structural Safety*, **32**(2), 112 - 123.
- [22] Yazgan U, Dazio A (2012): Post-earthquake damage assessment using residual displacements. *Earthquake Engineering and Structural Dynamics*, **41**(8), 1257-1276.
- [23] Ruiz-García J, Miranda E (2003): Inelastic displacement ratios for evaluation of existing structures. *Earthquake Engineering and Structural Dynamics*, **32**(8), 1237-1258.



- [24] Nagae T, Tahara K, Taizo M, et al. (2011): Design and instrumentation of the 2010 E-Defense four-story reinforced concrete and post-tensioned concrete buildings. *Technical Report PEER 2011/104*, Pacific Earthquake Engineering Research, Berkeley, USA.
- [25] Nagae T, Tahara K, Fukuyama K, et al. (2012): Test results of four-story reinforced concrete and post-tensioned concrete buildings: The 2010 E-Defense shaking table test. *Proceedings of Fifteenth World Conference on Earthquake Engineering*, Lisboa, Portugal.
- [26] CSI Perform 3D V5 (2011): *Nonlinear analysis and performance assessment for 3D structures*. CSI, Berkeley, California.
- [27] Paulay T, Priestley MJN (1992): *Seismic design of reinforced concrete and masonry buildings*. Wiley, New York.
- [28] Mander JB, Priestley MJN, Park R (1988): Theoretical stress-strain model for confined concrete. *Journal of structural engineering*, **114**(8), 1804-1826.
- [29] PEER/ATC (2010): Modeling and acceptance criteria for seismic design and analysis of tall buildings. *PEER/ATC 72-1 Report*, Applied Technology Council, Redwood City, CA, USA.
- [30] Tuna Z, Gavridou S, Wallace JW (2012): 2010 E-Defense four-story reinforced concrete and post-tensioned buildings - preliminary comparative study of experimental and analytical results. *Proceedings of Fifteenth World Conference on Earthquake Engineering*, Lisboa, Portugal.
- [31] ASCE (2005): Minimum design loads for buildings and other structures. *ASCE Standard ASCE/SEI 7-10*, Reston, VA.
- [32] PEER Center. NGA Strong Ground Motion Database. <<http://ngawest2.berkeley.edu/>>.
- [33] Campbell KW, Bozorgnia Y (2007): Campbell-Bozorgnia NGA ground motion relations for the geometric mean horizontal component of peak and spectral ground motion parameters. *Technical Report PEER 2007/02*, Pacific Earthquake Engineering Research, Berkeley, USA.
- [34] Hong HP, Goda K (2007): Orientation-dependent ground motion measure for seismic hazard assessment, *Bulletin of the Seismological Society of America*, **97**(5): 1525-1538.